Hindawi
International Journal of Aerospace Engineering
Volume 2018, Article ID 9571979, 10 pages
https://doi.org/10.1155/2018/9571979

Research Article

Study of Influential Factors of the Vibration Modal of the Rocket Equipment Bay and Structural Improvement Based on Finite Element Analysis

Chenghu Li, Guanlin Han, and Chunxu Duan

School of Aircraft Engineering, Nanchang Hangkong University, Nanchang 330063, China

Correspondence should be addressed to Chenghu Li; lichenghu111@126.com

Received 17 May 2018; Revised 24 July 2018; Accepted 6 August 2018; Published 4 September 2018

Academic Editor: Paolo Gasbarri

Copyright © 2018 Chenghu Li et al. This is an open access article distributed under the Creative Commons Attribution License, which permits unrestricted use, distribution, and reproduction in any medium, provided the original work is properly cited.

In this paper, the study focuses on influential factors of the vibration modal of the equipment bay of a carrier rocket and the structural improvement of the equipment bay by using finite element modal analysis. The finite element analysis focuses on the influences of the mass of the inertial bracket, the thickness of parts of the inertial bracket, and the stringer thickness on the first modal frequency of the equipment bay. As the analytical results show, the vibration displacement of mounting panels can be greatly reduced when the equipment bay is added with mass, and the vibration of the equipment bay with mass mainly occurs on the inertial bracket (without mass, the maximum vibration displacement occurs on the mounting panel); the top surface thickness of the inertial bracket has the maximum influence on the first modal frequency of the equipment bay, the stringer thickness and the side thickness of the inertial bracket have relatively high influence on the first modal frequency, the rib thickness of the inertial bracket has relatively low influence on the first modal frequency, and the beam thickness of the inertial bracket has the minimum influence on the first modal frequency.

1. Introduction

The equipment bay is an extremely important bay section of a carrier rocket, in which most of the rocket's instruments are mounted. The equipment bay has strict requirements for vibratory frequency. It requires a relatively high frequency of the first modal for avoiding sympathetic vibration and a relatively small vibration amplitude of its mounting panels. In the design of the equipment bay, finite element analysis is used to ensure that the structure of the equipment bay satisfies the requirements. Some applications of finite element analysis in simulation analyses of rockets have been presented. Choi et al. [1] evaluated the structural integrity and weight of the rocket motor with a hemispherical dome by analyzing the improved 2-D axisymmetric finite element model. Engberg and Korde [2] verified the possibility of 3-D full-scale finite element modeling by analyzing the two-dimensional finite element acoustic model of the fairing of a launch vehicle. Mahyari et al. [3] established a finite element model of the launch vehicle tank to analyze the effectiveness of the rotor crusher in reducing the critical height of propellant. Schwane and Xia [4] established a finite element model of the rocket engine nozzle to calculate the lateral load generated by the nozzle. Mense et al. [5] studied the thermal response of unprotected structural steel under solid rocket propellant flame by finite element thermal analysis. Howard et al. [6] verified the effect of the absorber in the rocket structure by analyzing the finite element model of the rectangular plate. Salvador and Xu [7] established a two-dimensional finite element model of the rocket burner with electrodes to analyze the influence of an electric field on flame combustion stability. Sim et al. [8] established finite element modeling techniques for computational modal analyses by considering the liquid propellant and flange joints of launch vehicles. Baldesi [9] introduced some studies that the dynamics analyses of various types of launch vehicles were executed by using finite element analysis. Hutchinson and Olds [10] estimated the structural weight of the propellant tank of a rocket by establishing a simplified beam finite element model. Marimuthu and Rao [11]carried out dynamic

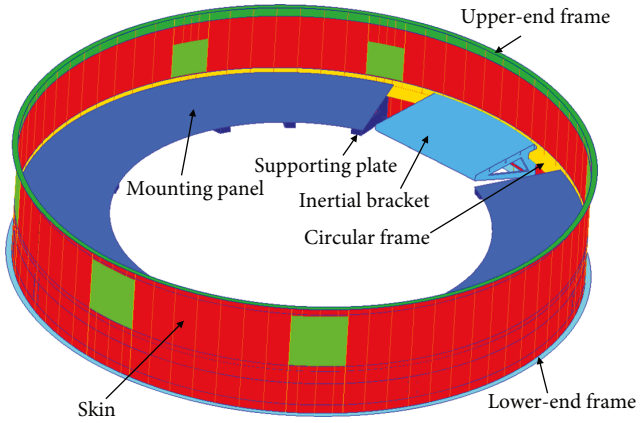

Figure 1: Geometry of the equipment bay.

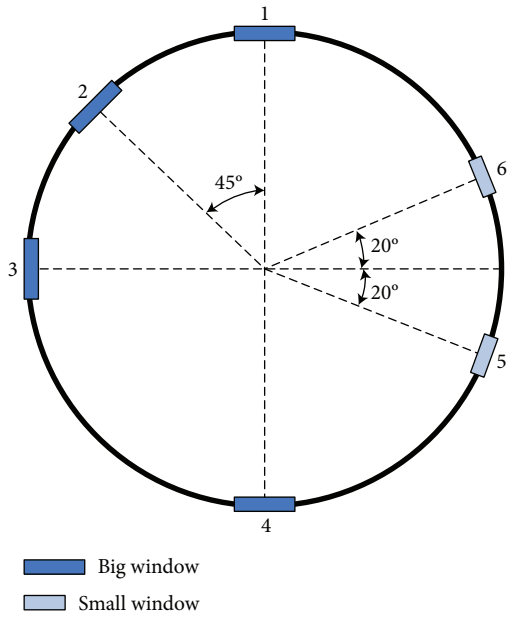

Figure 2: Location of windows.

analysis of the open cylindrical storage tank of a launch vehicle by means of finite element dynamic analysis. Roh and Kim [12] solved the trajectory optimization problem of a multistage launch vehicle by using an indirect time finite element method. Li and Zhang [13] researched the connection strength and slip characteristics of the rocket bolt by using finite element analysis. Elhefny and Liang [14] built a 2-D axisymmetric rocket gas turbine disk model to analyze the stress of the gas turbine disk. Zhang and Jiang [15] simulated the flight response of a rocket sled by using finite element coupling mechanical analysis. Chandana et al. [16] analyzed six mode shapes of the launch vehicle payload fairing structure by finite element analysis.

However, these studies focus on the application of finite element analysis in the simple rocket part structure, and the exhibit of finite element analysis in the complex rocket structures is less. This paper will present the vibration modal analysis of an equipment bay that has 7 parts and 572 thousand elements. The materials of the equipment bay include aluminum alloy, cast iron, carbon fiber composite laminates, and honeycomb sandwich. The parts in the finite element model of the equipment bay are linked by adhesive contacts, including in total 13 contact bodies that mutually adhere with each other. And the influence of some structural parameters of the equipment bay on its first modal and the structural improvement of the equipment bay will be investigated.

2. Finite Element Model of the Equipment Bay

The equipment bay includes 7 major parts such as the skin, upper-end frame, lower-end frame, supporting plate, mounting panel, circular frame, and inertial bracket, as shown in Figure 1. The skin is a reinforced cylindrical shell structure, with an outer diameter of 3000 mm and an overall height of 650 mm. It includes a cylindrical shell, stringer, window, and window cover. The skin is made of aluminum alloy. The function of stringers is to enhance the bearing capacity of the cylindrical shell, and the role of windows is to facilitate the installation and maintenance of equipment. The window includes a big window and a small window. The big window is a 300 mm × 300 mm square frame, and the small window is a 200 mm × 200 mm square frame. The lower-end of all the windows is 260 mm away from the lower-end of the skin. The location of the window on the skin is shown in Figure 2. Windows 1, 2, 3, and 4 are big windows and Windows 5 and 6 are small windows. The symmetry axis of Windows 1 and 4 coincides with the vertical symmetry axis. The symmetry axis of Window 3 coincides with the horizontal symmetry axis. The angle between the symmetry axis of Window 2 and the vertical symmetry axis is 45° and the angle between Windows 5 and 6 and the horizontal symmetry axis is 20°. The stringers have two types of cross sections, as shown in Figure 3. The parameters of the I-type stringer are $H_1 = 25$ mm, $W_1 = 20$ mm, $t_1 = 1.5$ mm, and $t_2 = 1.5$ mm. The parameters of the II-type stringer are $H_2 = 25$ mm, $W_2 = 20$ mm, $W_3 = 20$ mm, and $t_3 = 1.5$ mm. The number of I-type stringers and II-type stringers is 12 and 76, respectively. The cylindrical shell is simulated with a shell element of which the thickness is 1 mm. The stringer is simulated with a beam element. The skin finite element model is shown in Figure 4. In the figure, the 3-D beam is the result of the 3-D display of the 1-D beam element. The left and right sides of the window are reinforced by two I-type beams. The cylindrical shell of the skin is linked with stringers and a window cover by using merging nodes.

The inertial bracket is used to control the overall dynamic characteristics, which is made of cast iron as a whole. The finite element model of the inertial bracket is shown in Figure 5. In the figure, all the elements are plate shell elements. The top surface and rib have a thickness of 3.5 mm, the side surface and beam have a thickness of 2 mm, and the top surface and rib, top surface and beam, and rib and beam have the conodes on their intersection. The rib, beam, top surface, and side surface in the inertial bracket are linked with merging nodes, while the inertial bracket is linked with the skin and circular frame by adhesive contact. For the

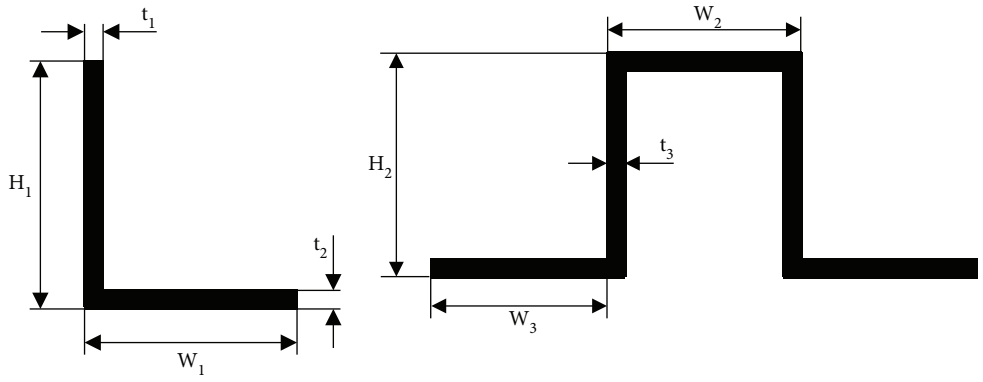

(a) Cross section of I-type stringer (b) Cross section of II-type stringer

Figure 3: Cross sections of I-type stringer and II-type stringer.

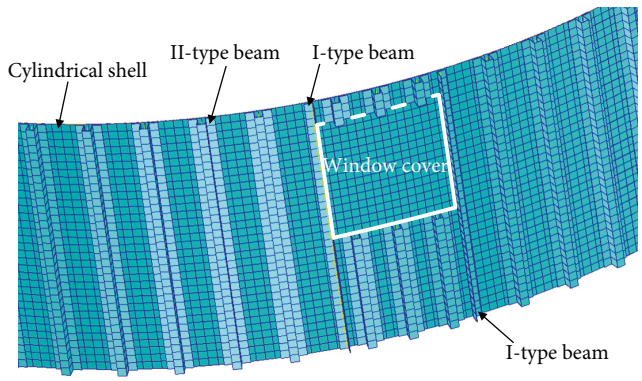

Figure 4: Finite element model of the skin.

successful setting of the adhesive contact, the distance between shell elements must be considered or the offset of the shell element is set or the distance between surfaces should be calculated when establishing the surfaces.

The supporting plate is used to support the mounting panel, and it is made of carbon fiber composite laminates. The stacking sequence of the laminates is $[45/0/-45/90]_{3S}$. Each layer has a thickness of 0.125 mm. The shell element is used for simulating the supporting plate. The finite element model of the supporting plate is shown in Figure 6. The blue surface of the supporting plate is in contact with the mounting panel, and its red surface and yellow surface are in contact with the skin and the circular frame, respectively.

The circular frame is used to enhance the stiffness and strength in the circumference direction of the skin. The finite element model of the circular frame is shown in Figure 7. The red surface of the circular frame is in contact with the skin, and its blue surface and yellow surface are in contact with the mounting panel and the supporting plate, respectively. The mounting panel is of a honeycomb sandwich. The upper and lower faces are carbon fiber laminates. The stacking sequence is $[45/0/-45/90]_S$. Each layer has a thickness of 0.125 mm. The middle sandwich is a 10 mm aluminum honeycomb. One 17-layer laminate is used to simulate the honeycomb sandwich. The mounting panel is in contact with the supporting plate and circular frame. The upper-end frame and lower-end frame are used to enhance the stiffness and strength of the upper and lower ends of the skin and are used to link the equipment bay with other bay sections, and their cross sections are both the "L" shape. The upper-end frame and the lower-end frame are in contact with the upper and lower ends of the skin, respectively. The overall finite element model of the equipment bay is shown in Figure 8. The model includes 4 materials: aluminum alloy, cast iron, CFRP (carbon fiber-reinforced polymer) tape, and aluminum honeycomb. Aluminum alloy and cast iron are isotropic materials, and the CFRP tape and aluminum honeycomb are 2-D orthotropic materials; their characteristics are shown in Table 1.

The parts of the equipment bay are linked by adhesive contact. In the finite element model, it is necessary to define the contact body and contact table. In the model, 13 contact bodies are defined in total: the portion of mounting panel that contacts with the circular frame is defined as Contact body 1, the portion of the mounting panel that contacts with the supporting plate is defined as Contact body 2, the portion of the inertial bracket that contacts with the skin is defined as Contact body 3, the portion of the inertial bracket that contacts with the circular frame is defined as Contact body 4, the portion of the skin that contacts with the upper-end frame is defined as Contact body 5, the portion of the skin that contacts with the lower-end frame is defined as Contact body 6 (the portion contacts also with the inertial bracket and supporting plate), the portion of the skin that contacts with the circular frame is defined as Contact body 7, the portion of the upper-end frame that contacts with the skin is defined as Contact body 8, the portion of the lower-end frame that contacts with the skin is defined as Contact body 9, the circular frame is defined as Contact body 10, the portion of the supporting plate that contacts with the mounting panel is defined as Contact body 11, the portion of the supporting plate that contacts with the skin is defined as Contact body 12, and the portion of the supporting plate that contacts with the circular frame is defined as Contact body 13. The two contact bodies in mutual contact are classified as the master and the slave. One contact body can be taken as the salve once only but as the master for n times. The contact table of the 13 contact bodies in mutual contact is shown in Table 2, where S represents the slave, M represents the

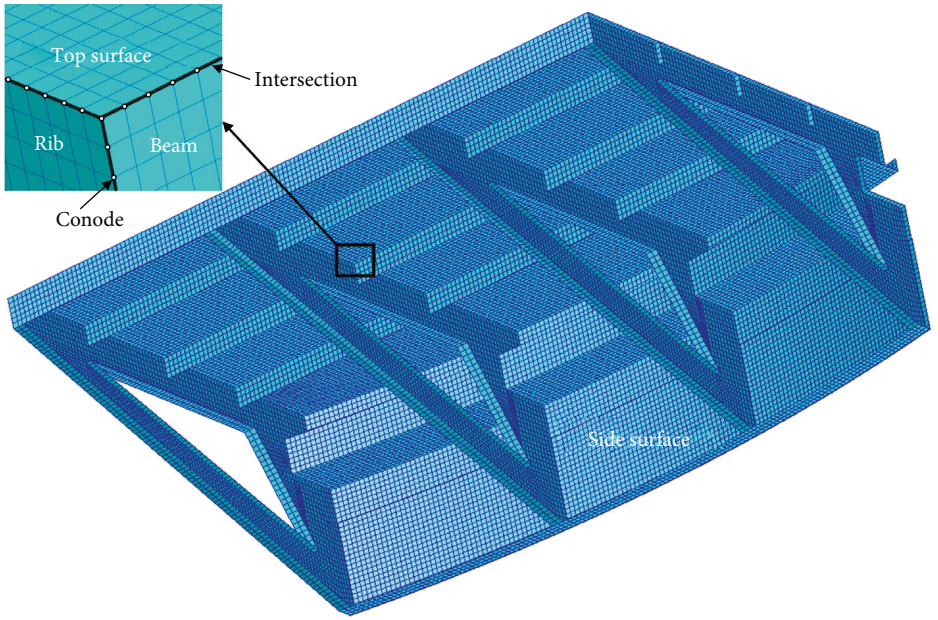

Figure 5: Finite element model of the inertial bracket.

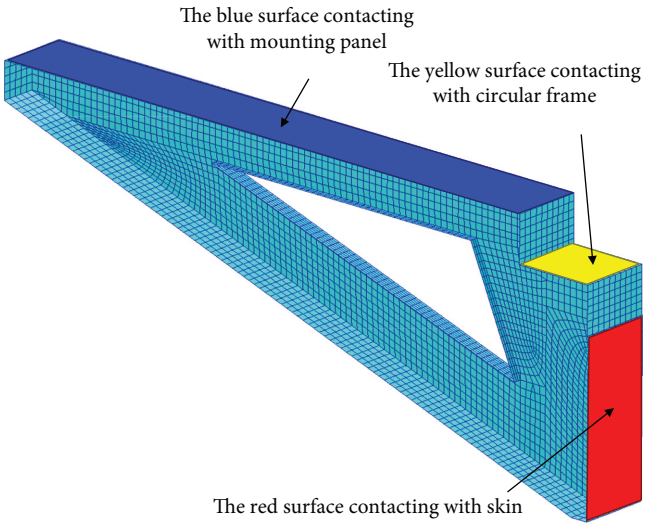

Figure 6: Finite element model of the supporting plate.

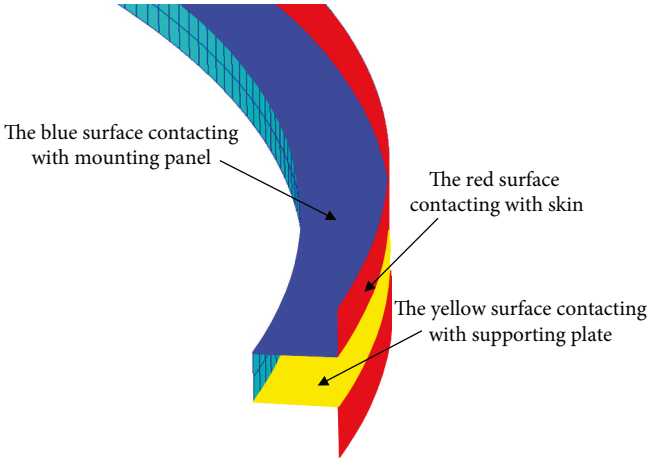

Figure 7: Finite element model of the circular frame.

master, and G represents the adhesive contact between contact bodies. Each row can have one G only, while each column can have more than one G. Column 6 has 3 Gs, indicating that Contact body 6 as the master is in adhesive contact with slave 3, slave 9, and slave 12. If two contact bodies are in contact with each other only, it is unnecessary to identify the master and the slave, for instance, the contact between Contact body 2 and Contact body 11.

3. Vibration Modal Analysis of Equipment Bay

The boundary conditions of the modal analysis of equipment bay are as follows: all freedoms of the nodes on the horizontal surface of the upper-end frame are restricted and all freedoms of the nodes on the horizontal surface of the lower-end frame are restricted. The first modal frequency of the equipment bay obtained by the finite element modal analysis is 52.487 Hz. The vibration shape is shown in Figure 9. The location of maximum vibration displacement is on the corner of the mounting panel, with the maximum value of 60.2 mm. Because the equipment is installed on the mounting panel and its excessive vibration displacement may cause damage to the equipment, it is necessary to reduce its vibration displacement. On the top surface of the inertial bracket, add three 20 kg masses, of which each represents the instrument with corresponding quality. The mass is defined with a 0D quality element, which is linked to the relevant nodes on the top surface by RBE3 (Rigid Body Element, Form3), as shown in Figure 10. With the masses added, the first modal frequency of the equipment bay is 28.816 Hz, and the vibration shape is shown in Figure 11. The area with relatively high vibration displacement is mainly on the inertial bracket,

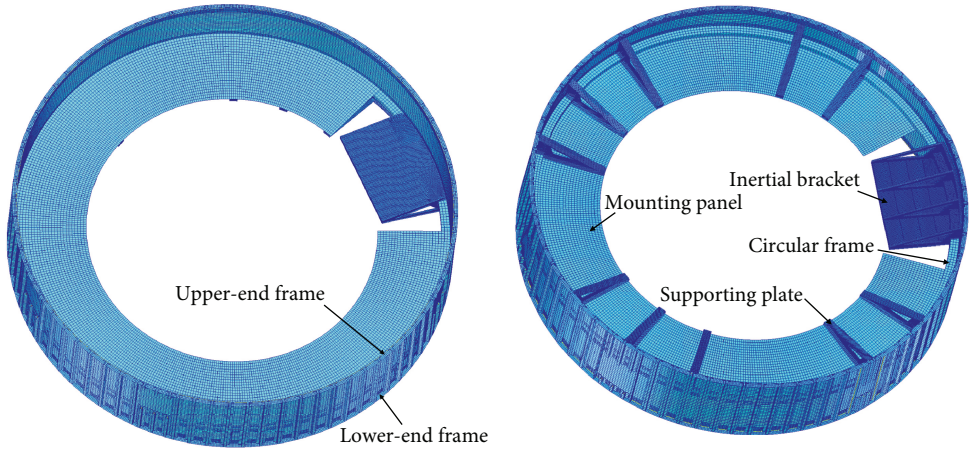

(a) Overall finite element model of the equipment bay (vertical view)

(b) Overall finite element model of the equipment bay (upward view)

Figure 8: Overall finite element model of the equipment bay.

Table 1: Material characteristics.

Aluminum alloy	Cast iron	CFRP tape	Aluminum honeycomb
		$E_{11} = 117$ GPa	$E_{11} = 120$ MPa
$E = 79$ GPa	$E = 160$ GPa	$E_{22} = 3$ GPa	$E_{22} = 120$ MPa
$\mu = 0.3$	$\mu = 0.26$	$G_{12} = 4$ GPa	$G_{12} = 11$ MPa
$\rho = 2600$ kg/m^3	$\rho = 7400$ kg/m^3	$\mu_{12} = 0.3$	$\mu_{12} = 0.3$
		$\rho = 1520$ kg/m^3	$\rho = 102$ kg/m^3

Table 2: Contact table of 13 contact bodies.

MS	1	2	3	4	5	6	7	8	9	10	11	12	13
1										G			
2											G		
3						G							
4										G			
5													
6													
7													
8					G								
9						G							
10							G						
11		G											
12						G							
13										G			

with the maximum value as 5.32 mm (being 8.8% of the maximum value before the mass is added). The vibration displacement of the two corners of the mounting panel is also relatively high. In order to reduce further the vibration displacement of the mounting panel, one supporting plate is added at the two sides of the mounting panel, so that the first modal frequency of the equipment bay becomes 29.615 Hz, with the vibration shape as shown in Figure 12. The area with

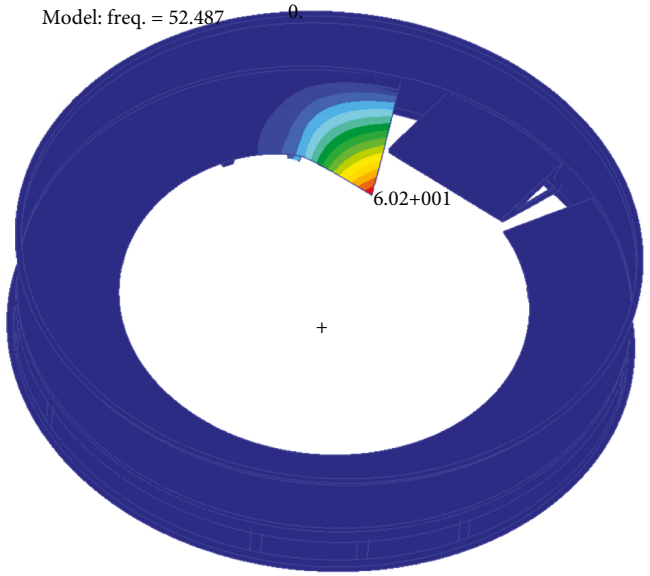

Figure 9: First modal shape of the equipment bay.

relatively high vibration displacement is mainly on the inertial bracket, with the maximum value as 5.19 mm.

In order to simulate more truly the vibration of the equipment bay in the rocket, extend the upper end and lower end of the skin by 200 mm (to reduce the influence of the boundary effect on the result). The first modal frequency of the extended equipment bay is 26.855 Hz; the vibration shape is shown in Figure 13. The area with relatively high vibration displacement is mainly on the inertial bracket, with the maximum value as 5.38 mm.

From the foregoing finite element analysis, it is known that the vibration of the equipment bay with the mass mainly occurs on the inertial bracket and its surrounding area, and thus, the influence of the following parameters on the first modal frequency of the equipment bay is further studied: the bracket top surface (as shown in Figure 14(a)) thickness T_1, the bracket rib (as shown in Figure 14(b)) thickness T_2,

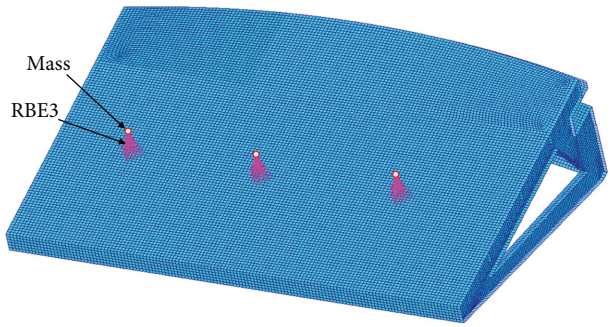

Figure 10: Mass on the inertial bracket.

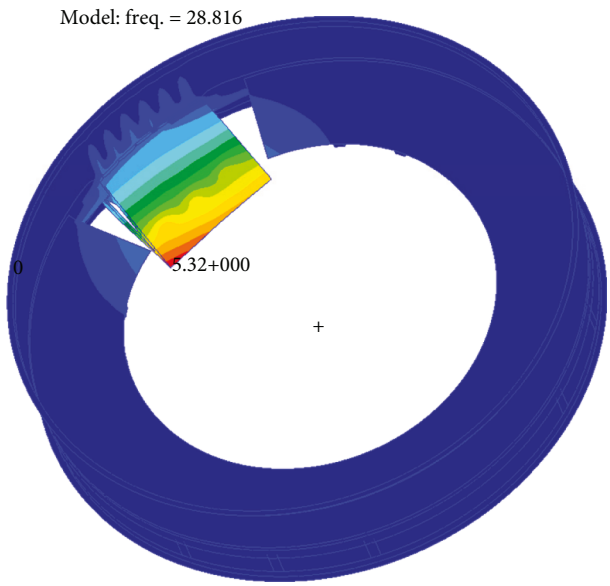

Figure 11: First modal shape of the equipment bay (with mass).

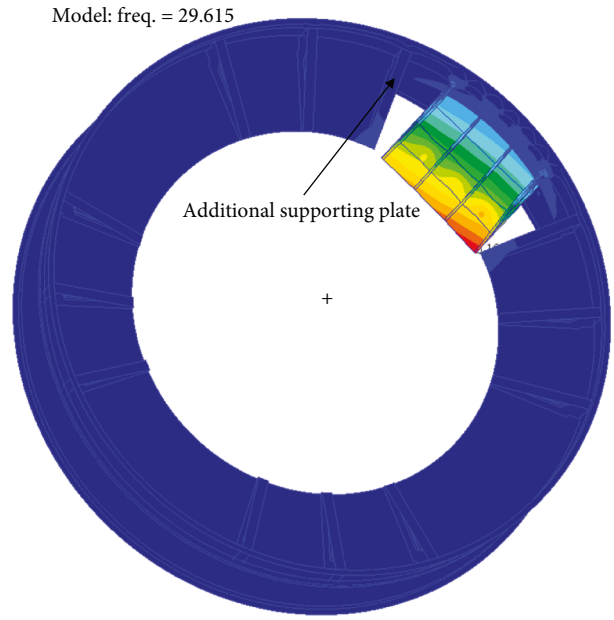

Figure 12: First modal shape of the equipment bay (with additional supporting plates).

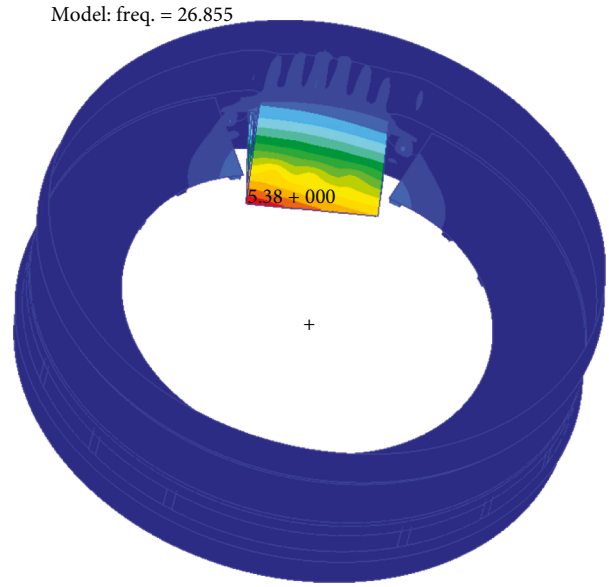

Figure 13: First modal shape of the equipment bay (extended).

the bracket side surface (as shown in Figure 14(c)) thickness T_3, the bracket beam (as shown in Figure 14(d)) thickness T_4, and the stringer (the relevant 6 stringers on the bracket side) thickness T_5. The initial value of these thicknesses is 3.5 mm for T_1, 3.5 mm for T_2, 2 mm for T_3, 2 mm for T_4, and 1.5 mm for T_5.

In order to study the influence of each parameter on the first modal of the equipment bay, keep 4 parameters unchanged and change one of them. Change T_1 (with the changing range of 2–4.5 mm) and keep the other 4 parameters unchanged. The influence of T_1 on the first modal frequency of the equipment bay is shown in Figure 15. The first modal frequency of the equipment bay increases with the increasing T_1. When T_1 is 2 mm, the frequency is 22.307 Hz. When T_1 is 4.5 mm, the frequency is 27.45 Hz. Change T_2 (with the changing range of 2–4.5 mm) and keep the other 4 parameters unchanged. The influence of T_2 on the first modal frequency of the equipment bay is shown in Figure 16. The first modal frequency of the equipment bay increases with the increasing T_2. When T_2 is 2 mm, the frequency is 26.518 Hz. When T_2 is 4.5 mm, the frequency is 26.853 Hz. Change T_3 (with the changing range of 1–4 mm) and keep the other 4 parameters unchanged. The influence of T_3 on the first modal frequency of equipment bay is shown in Figure 17. The first modal frequency of equipment bay increases with the increasing T_3. When T_3 is 1 mm, the frequency is 26.308 Hz. When T_3 is 4 mm, the frequency is 27.614 Hz. Change T_4 (with the changing range of 1–4 mm) and keep the other 4 parameters unchanged. The influence of T_4 on the first modal frequency of the equipment bay is shown in Figure 18. When T_4 is less than 2.5 mm, the first modal frequency of the equipment bay increases with increasing T_4. When T_4 is more than 2.5 mm, the first modal

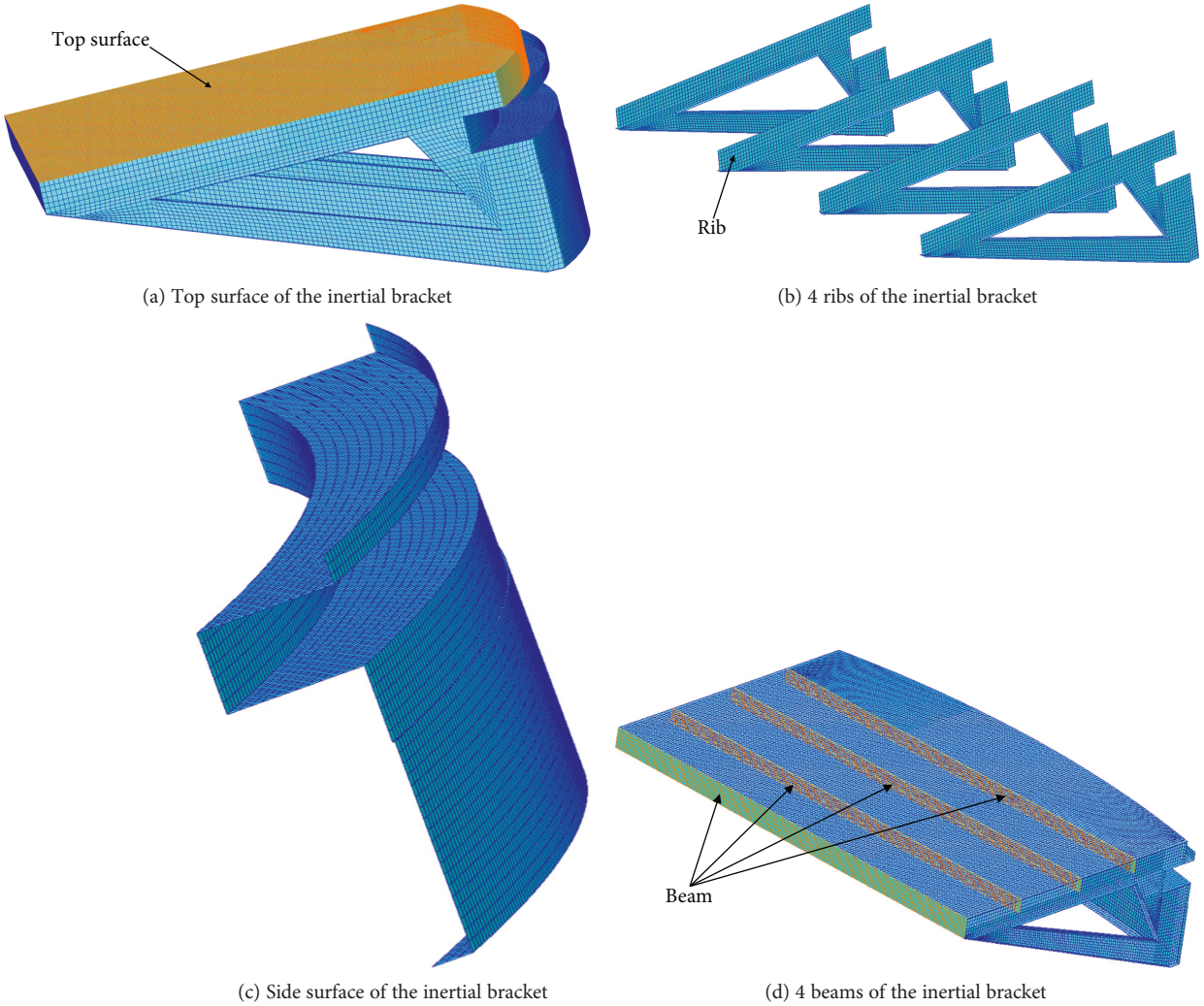

(a) Top surface of the inertial bracket

(b) 4 ribs of the inertial bracket

(c) Side surface of the inertial bracket

(d) 4 beams of the inertial bracket

Figure 14: 4 portions of the inertial bracket.

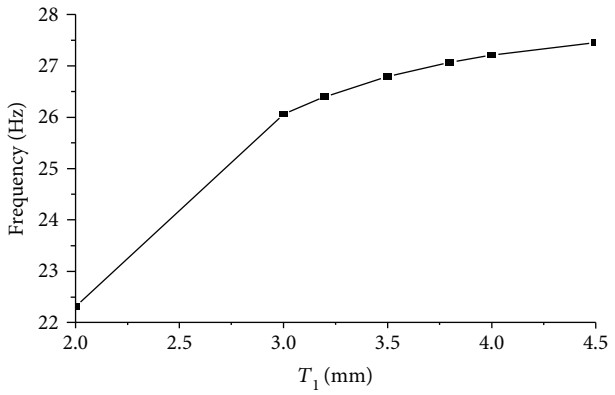

Figure 15: Influence of the inertial bracket top surface thickness on the first modal frequency of the equipment bay.

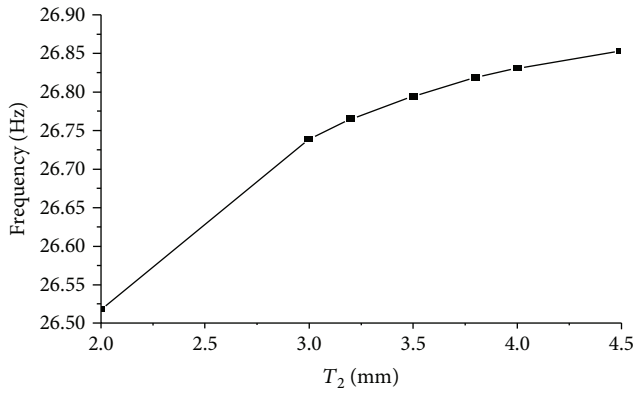

Figure 16: Influence of the inertial bracket rib thickness on the first modal frequency of the equipment bay.

frequency decreases with increasing T_4. When T_4 is 1 mm, the frequency is 26.704 Hz. When T_4 is 2.5 mm, the maximum frequency is 26.8 Hz. When T_4 is 4 mm, the frequency is 26.778 Hz. Change T_5 (with the changing range of 1-2 mm) and keep the other 4 parameters unchanged. The influence of T_5 on the first modal frequency of equipment bay is shown in Figure 19. The first modal frequency of the equipment bay increases with increasing T_5. When T_5 is

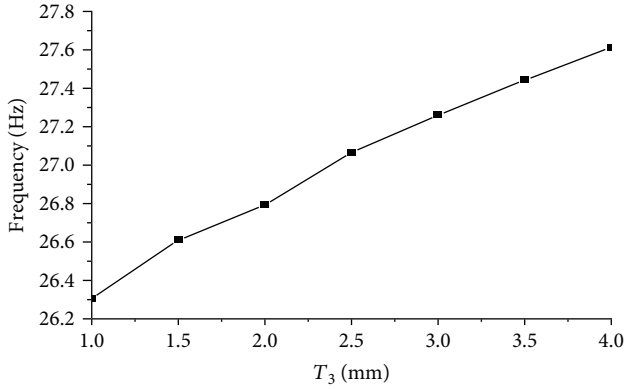

Figure 17: Influence of the inertial bracket side surface thickness on the first modal frequency of the equipment bay.

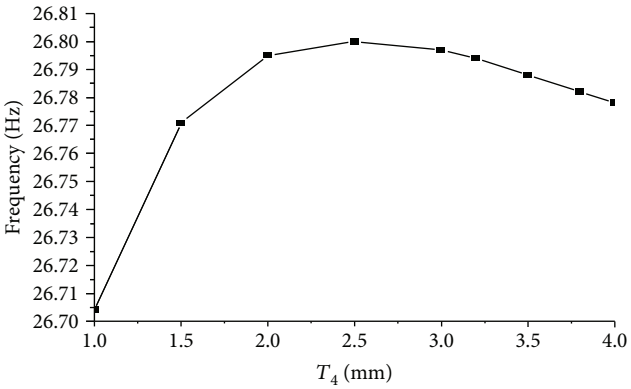

Figure 18: Influence of inertial bracket beam thickness on the first modal frequency of equipment bay.

1 mm, the frequency is 26.331 Hz. When T_5 is 2 mm, the frequency is 27.128 Hz.

From the foregoing figures and data, it is known that T_1 has the maximum influence on the first modal frequency of the equipment bay, the frequency increases with the increasing T_1, T_3 and T_5 have a relatively high influence on the first modal frequency of the equipment bay, the frequency increases as they increase, T_2 has a relatively low influence on the first modal frequency of the equipment bay, and T_4 has a minimum influence on the first modal frequency of the equipment bay. Thus, the vibration of the inertial bracket is simplified as the superimposition of two simple circumstances: Rod L is composed of Rod 1 and Rod 2. The shape of Rod L before the application of force is shown in Figure 20(a). When the stiffness of Rod 2 is very high and the stiffness of Rod 1 is relatively low, the shape of Rod L under the effect of Force F is shown in Figure 20(b), with Rod 2 not deformed and Rod 1 bending downward. When the stiffness of Rod 1 is very high and the stiffness of Rod 2 is relatively low, the deformation of Rod L under the effect of Force F is shown in Figure 20(c), with Rod 1 not deformed and Rod 2 bending. However, since the stiffness of Rod 1 and the stiffness of Rod 2 will not differ much, the deformation of Rod L under the effect of Force F is the composition of two

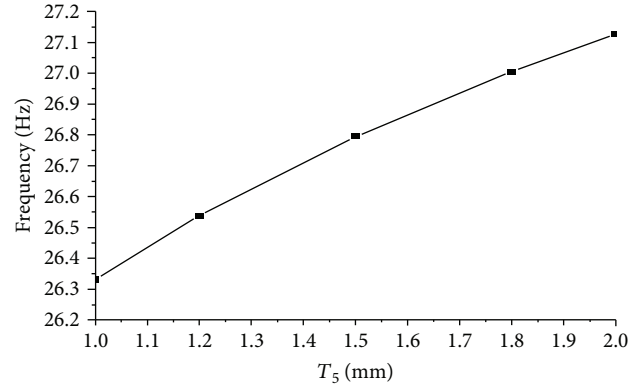

Figure 19: Influence of the stringer thickness on the first modal frequency of the equipment bay.

circumstances, as is consistent with the vibration of the inertial bracket (Rod 1 is equivalent to the top surface and Rod 2 is equivalent to the side surface). The first modal deformation of the top surface and side surface of the inertial bracket is shown in Figure 21. The comparison of the top surface and side surface before and after deformation proves the result of such composition.

Optimize comprehensively T_1, T_2, T_3, T_4, and T_5, with the optimizing target: under the condition that the first modal frequency of the equipment bay is more than 26 Hz, the weight of the equipment bay structure is the minimum. First, according to the influence of T_1, T_2, T_3, T_4, and T_5 on the first modal frequency of the equipment bay, adjust their changing range: the changing range of T_1 is 3–4.5 mm, the changing range of T_2 is 2–3.5 mm, the changing range of T_3 is 2-3 mm, the changing range of T_4 is 1–2 mm, and the changing range of T_5 is 1.2–2 mm. The result of comprehensive optimization is 3.2 mm for T_1, 2 mm for T_2, 2.1 mm for T_3, 1 mm for T_4, and 1.4 mm for T_5, the weight of the equipment bay is 162.8 kg, decreasing by 4.9 kg as compared with the initial weight.

4. Results and Discussion

Before inertial bracket is added with mass, the vibration of the equipment bay occurs mainly on the mounting panel, and the maximum vibration displacement is 60.2 mm; after the inertial bracket is added with mass, the vibration of the equipment bay occurs mainly on the inertial bracket, and the maximum vibration displacement is 5.32 mm (being 8.8% of the maximum value before mass is added), and with the inertial bracket added with mass, the maximum vibration displacement of the equipment bay is significantly reduced. By adding two supporting plates on both sides of the mounting panel, it can reduce effectively the vibration displacement of the mounting panel. In the further study, it is observed that the influence of the inertial bracket top surface thickness on the first modal frequency of the equipment bay is the highest. The influence of the inertial bracket side surface thickness and stringer thickness on the first modal frequency of the equipment bay is relatively high. The influence of the inertial bracket rib thickness on the first modal frequency of the

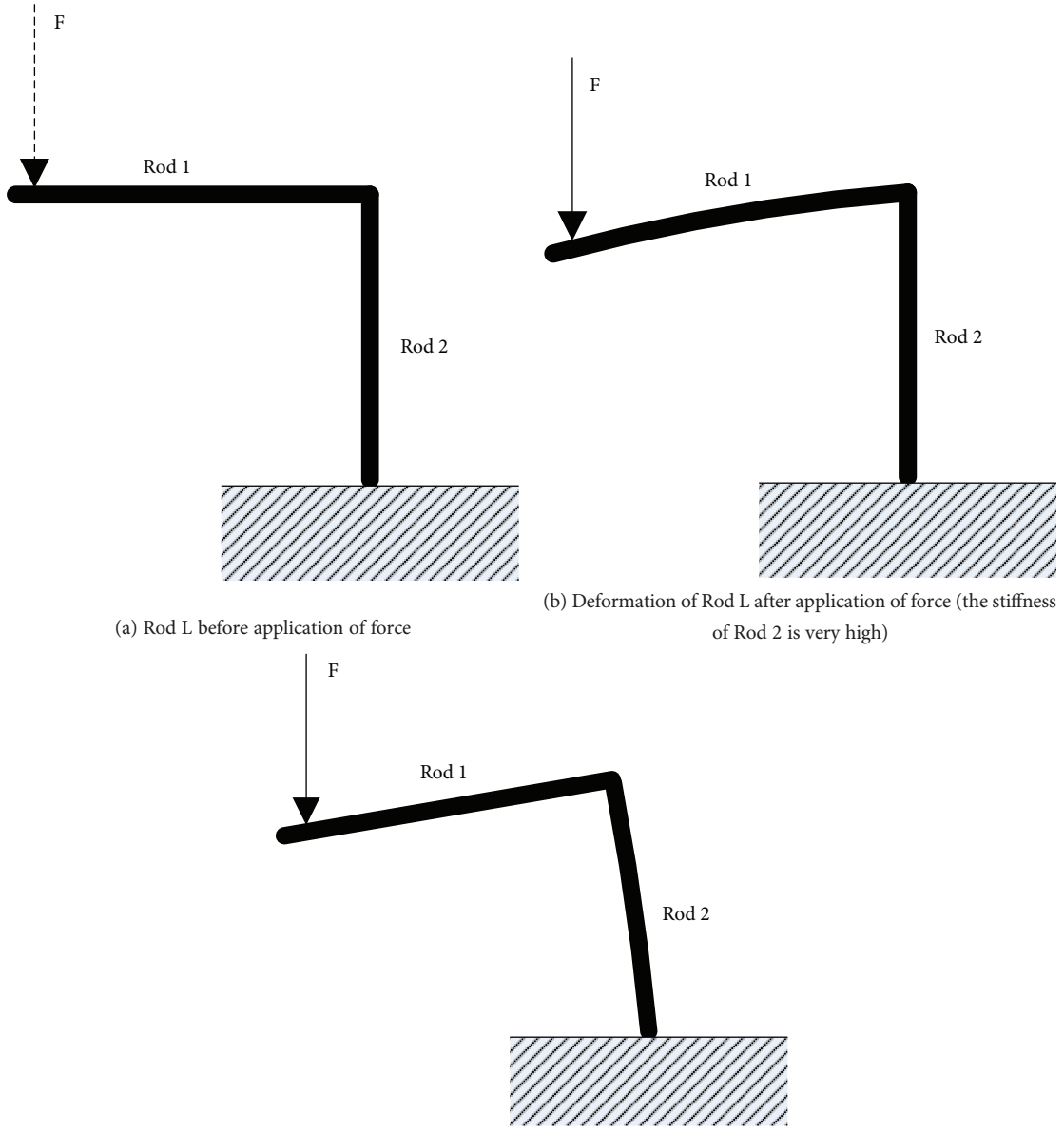

(a) Rod L before application of force

(b) Deformation of Rod L after application of force (the stiffness of Rod 2 is very high)

(c) Deformation of Rod L after application of force (the stiffness of Rod 1 is very high)

Figure 20: Deformation of Rod L.

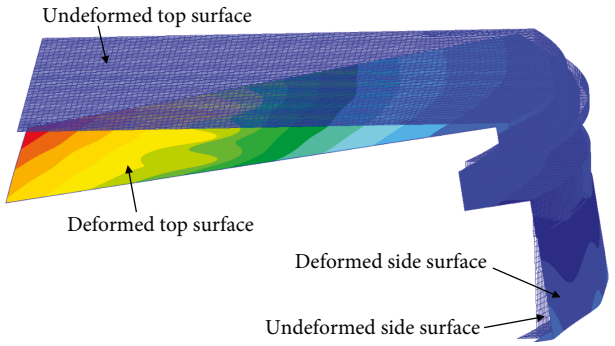

Figure 21: First modal deformation of the top surface and side surface of the inertial bracket.

equipment bay is relatively low, and the influence of the inertial bracket beam thickness on the first modal frequency of the equipment bay is the lowest. The vibration of the inertial bracket can be simplified as the deformation of Rod L (when the force is applied to Rod L). In engineering, the stiffness and vibration of the inertial bracket top surface (equivalent to Rod 1 of Rod L) is mostly studied, while the stiffness and vibration of the inertial bracket side surface (equivalent to Rod 2 of Rod L) is less studied. The analysis proves that studies on the stiffness and vibration of the top surface and side surface are all extremely important. The result of the comprehensive optimization of the equipment bay is 3.2 mm for T_1, 2 mm for T_2, 2.1 mm for T_3, 1 mm for T_4, and 1.4 mm for T_5; the weight of the equipment bay is 162.8 kg, decreasing by 4.9 kg as compared with the initial weight.

5. Conclusions

It can greatly reduce the vibration displacement of mounting panels when the inertial bracket is added with mass, and the vibration of the equipment bay with mass mainly occurs on the inertial bracket (without mass, the maximum vibration displacement occurs on the mounting panel). The top surface thickness of the inertial bracket has the maximum influence on the first modal frequency of the equipment bay, the stringer thickness and the side thickness of the inertial bracket have relatively high influence on the first modal frequency, the rib thickness of the inertial bracket has relatively low influence on the first modal frequency, and the beam thickness of the inertial bracket has the minimum influence on the first modal frequency. These results can be used to improve the equipment bay structure and decrease the weight of the equipment bay.

Data Availability

The data used to support the findings of this study are available from the corresponding author upon request.

Conflicts of Interest

The authors declare that there is no conflict of interest regarding the publication of this paper.

Acknowledgments

This work was supported by the Doctoral Foundation of Nanchang Hangkong University (EA201606185) and Innovation and Entrepreneurship Courses Training Project (KCPY1749 Foundation and Application of Finite Element Method).

References

[1] Y. G. Choi, K. B. Shin, and W. H. Kim, "A study on size optimization of rocket motor case using the modified 2D axisymmetric finite element model," *International Journal of Precision Engineering and Manufacturing*, vol. 11, no. 6, pp. 901–907, 2010.

[2] T. Engberg and U. A. Korde, "Modeling of the acoustic response of payload bays within launch vehicle fairings," *Journal of Spacecraft and Rockets*, vol. 50, no. 2, pp. 423–432, 2013.

[3] M. N. Mahyari, H. Karimi, H. Naseh, and M. Mirshams, "Numerical and experimental investigation of vortex breaker effectiveness on the improvement in launch vehicle ballistic parameters," *Journal of Mechanical Science and Technology*, vol. 24, no. 10, pp. 1997–2006, 2010.

[4] R. Schwane and Y. Xia, "Time-accurate CFD predictions and data validation for side load generation by flow-structure coupling in over-expanded rocket nozzles," *Journal of Mathematical Modelling and Algorithms*, vol. 4, no. 1, pp. 53–65, 2005.

[5] M. Mense, Y. Pizzo, C. Lallemand, J. C. Loraud, and B. Porterie, "Thermal response of an unprotected structural steel element exposed to a solid rocket propellant fire," *International Journal of Thermal Sciences*, vol. 105, pp. 195–205, 2016.

[6] C. Q. Howard, C. H. Hansen, and A. Zander, "Vibro-acoustic noise control treatments for payload bays of launch vehicles: discrete to fuzzy solutions," *Applied Acoustics*, vol. 66, no. 11, pp. 1235–1261, 2005.

[7] P. R. Salvador and K. G. Xu, "Direct current forcing of an atmospheric multiburner flame for rocket combustor emulation," *Journal of Spacecraft and Rockets*, vol. 55, no. 1, pp. 223–231, 2018.

[8] C. H. Sim, G. S. Kim, D. G. Kim, I. G. Kim, S. H. Park, and J. S. Park, "Experimental and computational modal analyses for launch vehicle models considering liquid propellant and flange joints," *International Journal of Aerospace Engineering*, vol. 2018, no. 2, 12 pages, 2018.

[9] G. Baldesi and M. Toso, "European Space Agency's launcher multibody dynamics simulator used for system and subsystem level analyses," *Ceas Space Journal*, vol. 3, no. 1-2, pp. 27–48, 2012.

[10] V. Hutchinson and J. Olds, "Estimation of launch vehicle propellant tank structural weight using simplified beam approximation," in *40th AIAA/ASME/SAE/ASEE Joint Propulsion Conference and Exhibit*, pp. 1–13, Fort Lauderdale, Florida, July 2004.

[11] R. Marimuthu and B. N. Rao, "An efficient finite element approach to examine the free vibration characteristics of liquid tankages in space launch vehicles," *Meccanica*, vol. 50, no. 5, pp. 1217–1226, 2015.

[12] W. Roh and Y. Kim, "Trajectory optimization for a multi-stage launch vehicle using time finite element and direct collocation methods," *Engineering Optimization*, vol. 34, no. 1, pp. 15–32, 2002.

[13] X. Li and X. Zhang, "The strength analysis of steel sunk screw connections in the rocket," *Acta Astronautica*, vol. 137, pp. 345–352, 2017.

[14] A. Elhefny and G. Liang, "Stress and deformation of rocket gas turbine disc under different loads using finite element modelling," *Propulsion and Power Research*, vol. 2, no. 1, pp. 38–49, 2013.

[15] J. H. Zhang and S. S. Jiang, "Definition of boundary conditions and dynamic analysis of rocket sled and turntable," *Applied Mechanics and Materials*, vol. 52-54, pp. 261–266, 2011.

[16] P. K. Chandana, S. B. Tiwari, and K. N. Vukkadala, "Numerical estimation of sound transmission loss in launch vehicle payload fairing," *Journal of The Institution of Engineers (India): Series C*, vol. 98, no. 4, pp. 471–478, 2017.

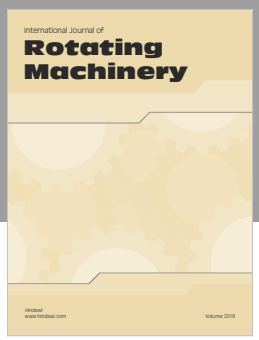

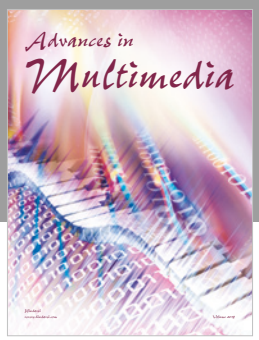

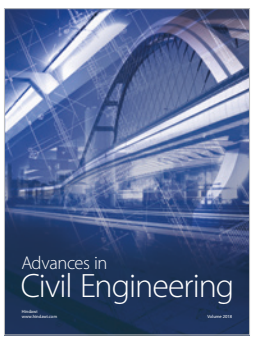

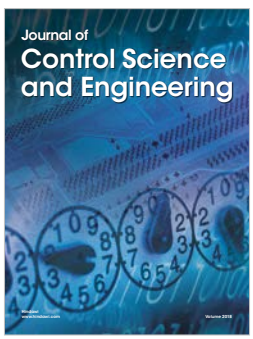

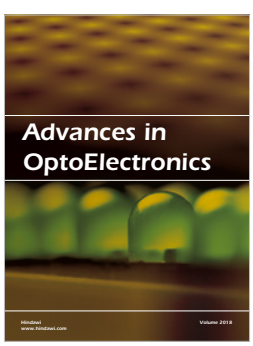

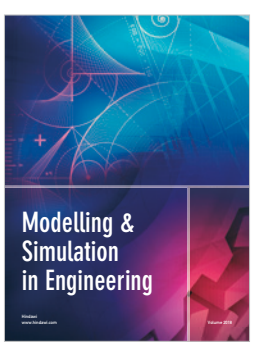

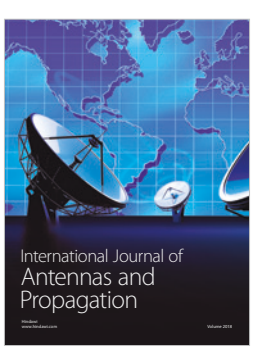

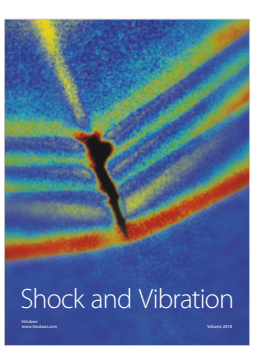

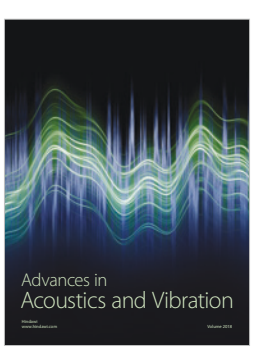

Hindawi

Submit your manuscripts at
www.hindawi.com